Output Feedback Control of an Underactuated Flying Inverted Pendulum

Weiming Yang[a], Joel Reis[a], Gan Yu[b] and Carlos Silvestre[a,c,*]

[a] *Faculty of Science and Technology, University of Macau, Macau, China*

[b] *School of Sensing Science and Engineering, School of Electronic Information and Electrical Engineering, Shanghai Jiao Tong University, Shanghai 200240, China*

[c] *Institute for Systems and Robotics, Instituto Superior Técnico, Universidade de Lisboa, Lisboa 1049-001, Portugal*

ARTICLE INFO

Keywords:
Nonlinear output feedback control
Underactuated dynamical systems
Flying inverted pendulum
Kalman filter

Abstract

This paper tackles the problem of trajectory tracking control for an inverted pendulum mounted on an underactuated unmanned aerial vehicle, operating under constant external disturbances. To model the pendulum's dynamics, a linear time-varying (LTV) system is first constructed. Within a stochastic framework, a Kalman filter is applied to this LTV system, shown to be uniformly completely observable, to obtain: estimates of the pendulum's angular velocity; estimates of the external disturbances; and noise-filtered measurements of the pendulum's orientation. A backstepping nonlinear controller is then designed, and it is analytically proven that the total error in the closed-loop system remains uniformly ultimately bounded. The effectiveness of the proposed strategy is demonstrated through simulations, with additional experimental results further validating its performance.

1. Introduction

A flying inverted pendulum (FIP) comprises a flying actuator, typically an underactuated unmanned aerial vehicle (UAV), and a balanced inverted pendulum. The latter is inherently unstable; maintaining its upright position is a classic problem in control theory that has long served as a benchmark for testing and refining new control strategies. The principles of an inverted pendulum are applied in various technologies, such as the balancing mechanisms in Segway vehicles Raffo, Ortega, Madero and Rubio (2015) and the dynamic jumping capabilities of wheeled bipedal robots Yu, Li, Tao, Feng, Zhang and Fu (2023). Inspired by these applications, FIPs can be utilized for ceiling inspections of tall buildings using specialized sensors mounted on the tip of the inverted pendulum Kocer, Tjahjowidodo, Pratama and Seet (2019). Additionally, the core framework of FIPs can evolve into complex parallel flying robot systems designed for specific manipulation and transportation tasks Liu, Fantoni and Chriette (2024). One of the most notable applications is in rocket landing control, as demonstrated in Jin, Wang, Yang and Mou (2020).

The control challenges in inverted pendulum systems primarily stem from the type of actuator used and the degrees of freedom they possess. For instance, the classical cart-pole system, which moves the pendulum using a cart Zhao and Spong (2001), and the Furuta pendulum, driven by a rotating actuator Aracil, Acosta and Gordillo (2013), have garnered considerable research attention. However, these systems typically feature only one or two degrees of freedom or are confined to planar motion, making their control complexities significantly less than those of the FIP system.

Achieving precise control of an inherently unstable FIP presents distinctive challenges: the system is underactuated (having fewer inputs than degrees of freedom) and exhibits strong couplings between its linear and angular dynamics. To address this problem, the work in Hehn and D'Andrea (2011) proposed a linearization method that separates the dynamics of the inverted pendulum from the rotational dynamics of the aerial vehicle. In Zhang, Hu, Gu and Wang (2017), an active disturbance rejection control law was developed to stabilize the inverted pendulum in two dimensions. It is important to note that both Hehn and D'Andrea (2011) and Zhang et al. (2017) use simplified dynamic models that assume the inverted pendulum is massless and do not provide proofs for the overall system stability.

In Yang, Yu, Reis and Silvestre (2024), the authors proposed a robust state-feedback nonlinear control approach for trajectory tracking of an FIP that does not involve any linearization. A major caveat of state-feedback control is that it requires measurements of all state variables, which is not always feasible or practical, especially for low-cost platforms with reduced dimensions. Indeed, the linear and angular velocities of an FIP can be challenging to measure.

To address the issue of unavailable state variables and noisy measurements, various observers and filtering techniques have been developed. These include high-gain observers (HGOs) Khalil (2017a), extended state observers (ESOs) Ran, Li and Xie (2021), extended high-gain observers (EHGOs) Khalil (2017b), and variations of the Kalman filter (KF) Zhou, Wang, Zhou, Wang and Chai

[⋆] This work was supported in part by the Macao Science and Technology Development Fund under Grants FDCT/0192/2023/RIA3 and 0059/2024/RIA1, in part by the University of Macau, Macau, China, under Projects MYRG2022-00205-FST, MYRG-GRG2023-00107-FST-UMDF and SRG2024-00012-FST, in part by the LARSyS FCT funding (DOI: 10.54499/LA/P/0083/2020, 10.54499/UIDP/50009/2020, and 10.54499/UIDB/ 50009/2020), in part by the National Natural Science Foundation of China under Grant 62403314, and in part by Startup Fund for Young Faculty at SJTU.

[*] Corresponding author

Email addresses: weiming.yang@connect.um.edu.mo (W. Yang); joelreis@um.edu.mo (J. Reis); sjtuganyu@sjtu.edu.cn (G. Yu); csilvestre@um.edu.mo (C. Silvestre)

(2020). The design of observers is particularly important when dealing with unknown exogenous disturbances and model parametric uncertainty. In the specific case of an underactuated UAV, the work in Kong, Reis, He and Silvestre (2023) reports a nonlinear control strategy that incorporates estimates obtained from an ESO into the backstepping design, with subsequent experimental verification attesting to its advantages and usefulness. For trajectory tracking problems involving an FIP, only a few studies have incorporated state observers into their designs. The work presented in Martinez-Vasquez, Castro-Linares, Rodríguez-Mata and Sira-Ramírez (2023) is highlighted here, where an ESO is designed based on a linearization of the FIP model, with its estimates used by an active disturbance rejection controller for trajectory tracking. It is also worth noting, although in a different but related context, the original work in Hofer, Muehlebach and D'Andrea (2023), which proposes a linear-quadratic regulator to stabilize a novel inverted pendulum design. The KF is used there to estimate states that are not directly measured and to compensate for communication delays.

The key highlights and contributions of this paper are summarized as follows:

1) Estimating unknown states in the FIP system presents a challenge due to its underactuated nature. This paper addresses the issue by introducing a linear time-varying (LTV) system, which is shown to be uniformly completely observable (UCO). Within a stochastic framework, a KF is employed to estimate the pendulum's angular velocity and the constant perturbations influencing both its linear and angular dynamics, using measurements of the pendulum's orientation.

2) Without relying on model linearization or other simplification techniques, a nonlinear output feedback control strategy is proposed that simultaneously achieves trajectory tracking for the FIP and stabilization of the pendulum's direction during movement.

3) Comprehensive three-dimensional trajectory tracking simulations and experimental results are presented to validate and demonstrate the effectiveness of the proposed solution. Compared to the work by Hehn and D'Andrea Hehn and D'Andrea (2011), the proposed approach shows improved tracking performance and enhanced robustness, thereby allowing for a broader range of practical applications.

2. Notation

The n-dimensional Euclidean space is denoted by $\mathbb{R}^n$. The set of unit vectors in $\mathbb{R}^3$ is denoted by $\mathbb{S}^2$. The symbols $\mathbf{I}$ and $\mathbf{0}$ represent the identity and zero matrices, respectively, both of appropriate dimensions. Transposition is denoted by $(\bullet)^\top$. For convenience, $\mathbf{e}_3 \triangleq [0\ 0\ 1]^\top$. The special orthogonal group of order three is represented by $\mathsf{SO}(3) \triangleq \{\mathbf{X} \in \mathbb{R}^{3\times3} : \mathbf{X}\mathbf{X}^\top = \mathbf{X}^\top\mathbf{X} = \mathbf{I},\ \det(\mathbf{X}) = 1\}$. $\mathbf{S}(\bullet)$ is a skew-symmetric matrix operator used in the vector cross product, i.e., $\mathbf{S}(\mathbf{a})\mathbf{c} = \mathbf{a}\times\mathbf{c}$, for $\mathbf{a}, \mathbf{c} \in \mathbb{R}^3$. The Euclidean norm is denoted by $\|\bullet\|$, and $\otimes$ denotes the Kronecker product. $\lambda_{\max}(\bullet)$ and $\lambda_{\min}(\bullet)$ represent the largest and smallest eigenvalues, respectively, of the argument matrix. Positive definiteness of a symmetric matrix $\mathbf{M}$ is indicated as $\mathbf{M} \succ \mathbf{0}$.

3. Preliminaries

This section provides the necessary preliminaries for the paper and formulates the control problem.

3.1. System Model

Consider a fixed inertial frame $\{I\}$ and a body-fixed frame $\{B\}$, with the origin of $\{B\}$ coinciding with the center of mass of the UAV. Both frames follow the North-East-Down (NED) axes convention. Throughout this paper, all vectors are defined in $\{I\}$ unless otherwise stated.

The FIP consists of two objects: a rigid-body UAV with mass $m_Q > 0$ and a load with mass $m_L > 0$, assumed to be concentrated at a single point, i.e., a point mass. They are connected by a rigid, massless pendulum of length $\ell > 0$.

The inertial coordinates of the UAV and the load are denoted by $\mathbf{p}_Q \in \mathbb{R}^3$ and $\mathbf{p}_L \in \mathbb{R}^3$, respectively. The corresponding linear velocities are given by $\mathbf{v}_Q \in \mathbb{R}^3$ and $\mathbf{v}_L \in \mathbb{R}^3$. The rotation matrix from $\{B\}$ to $\{I\}$ is denoted by $\mathbf{R} \in \mathsf{SO}(3)$. The direction of the pendulum, i.e., the unit vector pointing from the UAV to the load, is denoted by $\mathbf{q} \in \mathbb{S}^2$, such that

$$\ell\mathbf{q} = \mathbf{p}_L - \mathbf{p}_Q. \tag{1}$$

For simplicity of notation, define projection operators associated with $\mathbf{q}$ as

$$(\bullet)^{\parallel} \triangleq \mathbf{q}\mathbf{q}^\top(\bullet) \quad \text{and} \quad (\bullet)^{\perp} \triangleq -\mathbf{S}^2(\mathbf{q})(\bullet). \tag{2}$$

The angular velocity of the pendulum is denoted by $\boldsymbol{\omega} \in \mathbb{R}^3$.

The 8-degree-of-freedom configuration space of the FIP system is thus represented by $\mathbb{R}^3 \times \mathbb{S}^2 \times \mathsf{SO}(3)$. The corresponding kinematics equations are given by

$$\begin{cases} \dot{\mathbf{p}}_L = \mathbf{v}_L, & \text{(3a)} \\ \dot{\mathbf{q}} = \mathbf{S}(\boldsymbol{\omega})\mathbf{q}, \text{ and} & \text{(3b)} \\ \dot{\mathbf{R}} = \mathbf{R}\mathbf{S}(\boldsymbol{\Omega}), & \text{(3c)} \end{cases}$$

where $\boldsymbol{\Omega} \in \mathbb{R}^3$ represents the angular velocity of $\{B\}$ with respect to (w.r.t.) $\{I\}$, expressed in $\{B\}$. Notice that, according to (3b), the angular pendular motion is such that

$$\mathbf{q}^\top\boldsymbol{\omega} = 0. \tag{4}$$

The dynamic equations are given by (cf. Yang et al. (2024) or Lee, Sreenath and Kumar (2013)):

$$\begin{cases} \dot{\mathbf{v}}_L = \dfrac{1}{m_T}(\mathbf{f}+\mathbf{b})^{\parallel} - \dfrac{m_Q\ell}{m_T}\|\boldsymbol{\omega}\|^2\mathbf{q} + g\mathbf{e}_3, & \text{(5a)} \\ \dot{\boldsymbol{\omega}} = -\dfrac{1}{m_Q\ell}\mathbf{S}(\mathbf{q})(\mathbf{f}+\mathbf{b}), & \text{(5b)} \end{cases}$$

where $g > 0$ is the gravitational acceleration, $\mathbf{f} \in \mathbb{R}^3$ is the thrust force applied on the center of mass of the UAV, $m_T \triangleq m_Q + m_L$, and $\mathbf{b} \in \mathbb{R}^3$ accounts for unknown constant disturbances, such as wind, and may also include terms related to (additive) sensor noise. Define $\mathbf{r}_3 \triangleq \mathbf{R}\mathbf{e}_3 \in \mathbb{S}^2$, such that, in view of the underactuated nature of the UAV, one has $\mathbf{f} \triangleq -T\mathbf{r}_3$, with $T \triangleq \|\mathbf{f}\|$ being the net thrust generated only along the (vertical) z-axis of $\{B\}$.

3.2. Problem Statement

Consider a reference trajectory, denoted by $\mathbf{p}_{Ld} \in \mathbb{R}^3$, that is a curve of class at least C^5 with bounded derivatives. The goal is to design control laws for T and $\boldsymbol{\Omega}$ such that, in the presence of unknown constant perturbations $\mathbf{b}$, and without measurements of $\mathbf{v}_L$ and $\boldsymbol{\omega}$, the position $\mathbf{p}_L$ converges to the neighborhood of $\mathbf{p}_{Ld}$.

4. State Observer Design

In this section, the attitude subsystem of the FIP is represented as an LTV system, and an observability analysis of the proposed model is performed. A KF is subsequently designed in Section 4.3 to estimate the unmeasured states.

4.1. Linear Time-varying System Design

Start by defining the state and output vectors as

$$\boldsymbol{x}(t) \triangleq \begin{bmatrix}\mathbf{q}^\top(t) & \boldsymbol{\omega}^\top(t) & \frac{1}{m_Q\ell}\mathbf{b}^\top\end{bmatrix}^\top \in \mathbb{R}^9 \text{ and} \tag{6}$$

$$\boldsymbol{y}(t) \triangleq \begin{bmatrix}\mathbf{q}^\top(t) & 0\end{bmatrix}^\top \in \mathbb{R}^4, \tag{7}$$

respectively. Then, based on (3b) and (5b), and according to (6) and (7), an LTV system can be formulated as

$$\begin{cases}\dot{\boldsymbol{x}}(t) = \mathbf{A}(t)\boldsymbol{x}(t) + \mathbf{B}(t)\boldsymbol{u}(t) + \mathbf{w}(t),\\ \boldsymbol{y}(t) = \mathbf{C}(t)\boldsymbol{x}(t) + \mathbf{n}(t),\end{cases} \tag{8}$$

where the input signal is defined as

$$\boldsymbol{u}(t) \triangleq \frac{1}{m_Q\ell}\mathbf{f}(t) \in \mathbb{R}^3, \tag{9}$$

and the state-space matrices are given by

$$\mathbf{A}(t) = \begin{bmatrix}\mathbf{0} & -\mathbf{S}(\mathbf{q}(t)) & \mathbf{0}\\ \mathbf{0} & \mathbf{0} & -\mathbf{S}(\mathbf{q}(t))\\ \mathbf{0} & \mathbf{0} & \mathbf{0}\end{bmatrix} \in \mathbb{R}^{9\times 9}, \tag{10}$$

$$\mathbf{B}(t) = \begin{bmatrix}\mathbf{0} & \mathbf{S}(\mathbf{q}(t)) & \mathbf{0}\end{bmatrix}^\top \in \mathbb{R}^{9\times 3}, \tag{11}$$

$$\mathbf{C}(t) = \begin{bmatrix}\mathbf{I} & \mathbf{0} & \mathbf{0}\\ \mathbf{0} & \mathbf{q}^\top(t) & \mathbf{0}\end{bmatrix} \in \mathbb{R}^{4\times 9}. \tag{12}$$

Here, $\mathbf{w} \sim \mathcal{N}(\mathbf{0}, \mathcal{Q})$ and $\mathbf{n} \sim \mathcal{N}(\mathbf{0}, \mathcal{R})$ represent the (uncorrelated) process and observation noises, both assumed to be extracted from zero mean multivariate normal distributions with covariances $\mathcal{Q} \in \mathbb{R}^{9\times 9}$ and $\mathcal{R} \in \mathbb{R}^{4\times 4}$, respectively.

Note that the *zero* in (7) represents a virtual measurement based on the inherent geometric constraint given by (4). This decision will be helpful in analyzing the observability of the linear state equation (8).

4.2. Observability Analysis

The observability of the LTV system (8) is examined here. The transition matrix $\boldsymbol{\Phi}(t, t_0) \in \mathbb{R}^{9\times 9}$ associated with the state transition matrix $\mathbf{A}(t)$ in (10), which can be computed through the Peano-Baker series, is given by

$$\boldsymbol{\Phi}(t, t_0) = \begin{bmatrix}\mathbf{I} & -\int_{t_0}^{t}\mathbf{S}(\mathbf{q}(\tau))d\tau & \int_{t_0}^{t}\mathbf{S}(\mathbf{q}(\tau))\int_{t_0}^{\tau}\mathbf{S}(\mathbf{q}(\sigma))d\sigma d\tau\\ \mathbf{0} & \mathbf{I} & -\int_{t_0}^{t}\mathbf{S}(\mathbf{q}(\tau))d\tau\\ \mathbf{0} & \mathbf{0} & \mathbf{I}\end{bmatrix}. \tag{13}$$

The observability Gramian associated with the pair ($\mathbf{A}(t)$, $\mathbf{C}(t)$), denoted here by $\boldsymbol{W}(t_0, t_f) \in \mathbb{R}^{9\times 9}$, is defined as

$$\boldsymbol{W}(t_0, t_f) \triangleq \int_{t_0}^{t_f}\boldsymbol{\Phi}^\top(t, t_0)\mathbf{C}(t)^\top\mathbf{C}(t)\boldsymbol{\Phi}(t, t_0)dt. \tag{14}$$

Definition 1. *(Jazwinski (2007), Uniform Complete Observability). Given constants $\alpha_1, \alpha_2, \beta > 0$, the continuous-time LTV system (8) is UCO if and only if*

$$\alpha_1\mathbf{I} \le \boldsymbol{W}(t, t+\beta) \le \alpha_2\mathbf{I}, \quad \forall t \ge t_0. \tag{15}$$

The following proposition, a particular case of Proposition 4.2 developed in Batista, Silvestre and Oliveira (2011), is useful in the sequel.

Proposition 1. *Let $\mathbf{g}(t) : [t_0, t_f] \subset \mathbb{R} \to \mathbb{R}^3$ be a continuous and two times differentiable function on $\phi \triangleq [t_0, t_f]$, where $T \triangleq t_f - t_0 > 0$, and such that $\mathbf{g}(t_0) \ge 0$. Further assume that $\ddot{\mathbf{g}}(t)$ is bounded on ϕ. If there exist $\rho > 0$ and $t_1 \in \phi$ such that $\|\dot{\mathbf{g}}(t_1)\| \ge \rho$, then there exist $0 < t_2 < T$ and $\theta > 0$ such that $\|\mathbf{g}(t_0 + t_2)\| \ge \theta$.*

Theorem 1. *The continuous-time LTV system (8), with $\mathbf{f}$ uniformly bounded, is UCO on $\phi \triangleq [t, t+\beta]$, for some $\beta > 0$, if the direction of the pendulum is not constant, i.e.,*

$$\exists\tau \in \phi \;:\; \mathbf{S}(\mathbf{q}(t))\mathbf{q}(\tau) \ne \mathbf{0}, \quad \forall t \ge t_0. \tag{16}$$

Proof. Start by defining a vector $\boldsymbol{d} \triangleq \begin{bmatrix}\boldsymbol{d}_1^\top & \boldsymbol{d}_2^\top & \boldsymbol{d}_3^\top\end{bmatrix}^\top \in \mathbb{R}^9$, with $\boldsymbol{d}_1, \boldsymbol{d}_2, \boldsymbol{d}_3 \in \mathbb{R}^3$, such that $\|\boldsymbol{d}\| = 1$. Bear in mind that $t \ge t_0$ represents an arbitrary moment of time, with t_0 representing the initial time of the simulation/experiment, typically set to zero for convenience. Let τ be an auxiliary quantity denoting another instance of time, belonging to the interval ϕ. Therefore, according to (14), one can write

$$\boldsymbol{d}^\top\boldsymbol{W}(t, t+\beta)\boldsymbol{d} = \int_t^{t+\beta}\|\mathbf{g}(\tau, t)\|^2 d\tau, \tag{17}$$

where, for all $\tau \in \phi$ and $t \ge t_0$, $\mathbf{g}(\tau, t) \in \mathbb{R}^4$ is given by

$$\mathbf{g}(\tau, t) = \begin{bmatrix}\boldsymbol{d}_1 - \int_t^{\tau}\mathbf{S}(\mathbf{q}(\sigma))\boldsymbol{d}_2 d\sigma \ldots\\ \ldots + \int_t^{\tau}\mathbf{S}(\mathbf{q}(\sigma))\int_t^{\sigma}\mathbf{S}(\mathbf{q}(\upsilon))\boldsymbol{d}_3 d\upsilon d\sigma\\ \mathbf{q}^\top(\tau)\left(\boldsymbol{d}_2 - \int_t^{\tau}\mathbf{S}(\mathbf{q}(\sigma))\boldsymbol{d}_3 d\sigma\right)\end{bmatrix}. \tag{18}$$

Notice that (13) consists of terms that depend only on the unit vector $\mathbf{q}$. Therefore, since the integral over a finite interval of a bounded quantity is also finite, it follows that $\mathbf{\Phi}(t,t_0)$ is bounded as well. Moreover, $\mathbf{C}$, as shown in (12), is also a bounded matrix since its only time-varying term is a unit vector. Hence, according to (14), $W(t_0,t_f)$ is upper bounded. Then, based on (18), one has

$$\mathbf{g}(t,t) = \begin{bmatrix} \boldsymbol{d}_1 \\ \mathbf{q}^\top(t)\boldsymbol{d}_2 \end{bmatrix}, \quad \forall t \geq t_0, \tag{19}$$

meaning that for some $\|\boldsymbol{d}_1\| = \delta_1 > 0$ it must be $\|\mathbf{g}(t,t)\| \geq \delta_1$ for all $t \geq t_0$. Likewise, for some $\boldsymbol{d}_2$ not orthogonal to $\mathbf{q}(t)$, such that $|\mathbf{q}^\top(t)\boldsymbol{d}_2| = \delta_2 > 0$, it follows that $\|\mathbf{g}(t,t)\| \geq \delta_2$ for all $t \geq t_0$. Suppose then that $\boldsymbol{d}_1 = \mathbf{0}$ and that $\boldsymbol{d}_2$ is orthogonal to $\mathbf{q}(t)$, therefore implying $\|\mathbf{g}(t,t)\| = 0$, for all $t \geq t_0$.

Next, compute the first derivative of (18) w.r.t. τ, which, for all $\tau \in \phi$, results in

$$\frac{d\mathbf{g}(\tau,t)}{d\tau} = \begin{bmatrix} -\mathbf{S}(\mathbf{q}(\tau))\left(\boldsymbol{d}_2 - \int_t^\tau \mathbf{S}(\mathbf{q}(\sigma))\boldsymbol{d}_3 d\sigma\right) \\ -\mathbf{q}^\top(\tau)\mathbf{S}(\boldsymbol{\omega}(\tau))\left(\boldsymbol{d}_2 - \int_t^\tau \mathbf{S}(\mathbf{q}(\sigma))\boldsymbol{d}_3 d\sigma\right) \end{bmatrix}. \tag{20}$$

Evaluating (20) at $\tau = t$ yields

$$\left.\frac{d\mathbf{g}(\tau,t)}{d\tau}\right|_{\tau=t} = \begin{bmatrix} -\mathbf{S}(\mathbf{q}(t))\boldsymbol{d}_2 \\ -\mathbf{q}^\top(t)\mathbf{S}(\boldsymbol{\omega}(t))\boldsymbol{d}_2 \end{bmatrix}. \tag{21}$$

Because $\boldsymbol{d}_2$ is orthogonal to $\mathbf{q}(\tau)$, there must exist $\delta_3 = \|\mathbf{S}(\mathbf{q}(t))\boldsymbol{d}_2\| > 0$ such that $\left\|\left.\frac{d\mathbf{g}(\tau,t)}{d\tau}\right|_{\tau=t}\right\| \geq \delta_3$, for all $t \geq t_0$. Suppose then that $\boldsymbol{d}_2 = \mathbf{0}$. With $\boldsymbol{d}_1 = \boldsymbol{d}_2 = \mathbf{0}$, it must be $\|\boldsymbol{d}_3\| = 1$. Hence, it follows from (18) and (20) that

$$\mathbf{g}(\tau,t) = \begin{bmatrix} \int_t^\tau \int_t^\sigma \mathbf{S}(\mathbf{q}(\sigma))\mathbf{S}(\mathbf{q}(\upsilon))\boldsymbol{d}_3 d\upsilon d\sigma \\ -\mathbf{q}^\top(\tau)\int_t^\tau \mathbf{S}(\mathbf{q}(\sigma))\boldsymbol{d}_3 d\sigma \end{bmatrix} \tag{22}$$

and

$$\frac{d\mathbf{g}(\tau,t)}{d\tau} = \begin{bmatrix} \mathbf{S}(\mathbf{q}(\tau))\int_t^\tau \mathbf{S}(\mathbf{q}(\sigma))\boldsymbol{d}_3 d\sigma \\ \mathbf{q}^\top(\tau)\mathbf{S}(\boldsymbol{\omega}(\tau))\int_t^\tau \mathbf{S}(\mathbf{q}(\sigma))\boldsymbol{d}_3 d\sigma \end{bmatrix}. \tag{23}$$

In view of the second row of (22) and first row of (23), observe that the term $\int_t^\tau \mathbf{S}(\mathbf{q}(\sigma))\boldsymbol{d}_3 d\sigma = -\mathbf{S}(\boldsymbol{d}_3)\int_t^\tau \mathbf{q}(\sigma)d\sigma$ cannot be simultaneously collinear and orthogonal to $\mathbf{q}(\tau)$. Hence, it follows that there must exist $\delta_4 > 0$ such that, for all $\tau \in \phi$ and $t \geq t_0$, if $\int_t^\tau \mathbf{q}(\sigma)d\sigma$ is not collinear to $\boldsymbol{d}_3$ then

$$\begin{aligned} &\left\|\int_t^\tau \mathbf{S}(\mathbf{q}(\sigma))\boldsymbol{d}_3 d\sigma\right\| = \delta_4 \implies \dots \\ &\dots \implies \|\mathbf{g}(\tau,t)\| \geq \delta_4 \vee \left\|\frac{d\mathbf{g}(\tau,t)}{d\tau}\right\| \geq \delta_4. \end{aligned} \tag{24}$$

Suppose then that $\int_t^\tau \mathbf{q}(\sigma)d\sigma$ is collinear with $\boldsymbol{d}_3$ for all $\tau \in \phi$, with $\|\boldsymbol{d}_3\| = 1$. With (16) holding true, the direction of $\mathbf{q}(\tau)$ cannot remain constant in ϕ. Therefore, (24) is always true unless $\boldsymbol{d}_3 = \mathbf{0}$, but this would contradict the fact that $\|\boldsymbol{d}_3\| = 1$. This means, on account of (20) and its derivative being uniformly bounded, that by using Proposition (1) there must exist constants α_1, α_2 and β such that $\alpha_1 \leq \boldsymbol{d}^\top \boldsymbol{W}(t,t+\beta)\boldsymbol{d} \leq \alpha_2$, for all $t \geq t_0$. □

Remark 1. *In theory, the vertical direction of the pendulum, expressed by the column vector* $[0\ 0\ -1]^\top$, *is an unstable equilibrium point for the FIP system. However, Theorem 1 requires the direction to change only once in a certain interval. Simply put, as long as the FIP system does not initiate the maneuver at the equilibrium point, in practice the LTV system* (8) *will always be observable.*

4.3. Kalman Filter as State Observer

Similarly to the definition in (6), let the system state estimate be denoted by $\hat{\boldsymbol{x}}(t) \in \mathbb{R}^9$. More specifically

$$\hat{\boldsymbol{x}}(t) \triangleq \begin{bmatrix} \hat{\mathbf{q}}^\top(t) & \hat{\boldsymbol{\omega}}^\top(t) & \frac{1}{m_Q \ell}\hat{\mathbf{b}}^\top(t) \end{bmatrix}^\top. \tag{25}$$

The Kalman-Bucy filter is selected as a natural estimator for (8). Its classical structure is given by

$$\begin{aligned} \dot{\hat{\boldsymbol{x}}}(t) &\triangleq \mathbf{A}(t)\hat{\boldsymbol{x}}(t) + \mathbf{B}(t)\boldsymbol{u}(t) + \boldsymbol{\mathcal{K}}(t)\big(\boldsymbol{y}(t) - \mathbf{C}(t)\hat{\boldsymbol{x}}(t)\big) && \text{(26a)} \\ \boldsymbol{\mathcal{K}}(t) &\triangleq \boldsymbol{\mathcal{P}}(t)\mathbf{C}^\top(t)\boldsymbol{\mathcal{R}}^{-1} && \text{(26b)} \\ \dot{\boldsymbol{\mathcal{P}}}(t) &\triangleq \mathbf{A}(t)\boldsymbol{\mathcal{P}}(t) + \boldsymbol{\mathcal{P}}(t)\mathbf{A}^\top(t) + \boldsymbol{\mathcal{Q}} - \boldsymbol{\mathcal{K}}(t)\boldsymbol{\mathcal{R}}\boldsymbol{\mathcal{K}}^\top(t) && \text{(26c)} \end{aligned}$$

where $\boldsymbol{\mathcal{Q}}$ and $\boldsymbol{\mathcal{R}}$ are positive definite matrices (assumed to be constant), originally introduced to characterize the noises in (8), $\boldsymbol{\mathcal{K}}(t) \in \mathbb{R}^{9\times3}$ is the time-varying Kalman gain, and $\boldsymbol{\mathcal{P}}(t) \in \mathbb{R}^{9\times9}$ denotes the positive definite covariance of the state estimation error obtained from the Riccati differential equation (26c). The initial conditions $\hat{\boldsymbol{x}}(t_0)$ and $\boldsymbol{\mathcal{P}}(t_0) \succ \mathbf{0}$ are selected by the user.

Remark 2. *The KF described in* (26) *operates under the assumption that the disturbance term* $\mathbf{b}$ *remains constant over time. Accounting for time-varying behavior would require explicit knowledge of the time derivative* $\dot{\mathbf{b}}(t)$, *which complicates the filter design. However, by appropriately increasing the relevant entries in the process noise covariance matrix* $\boldsymbol{\mathcal{Q}}$, *the filter can accommodate stochastic variations in* $\mathbf{b}(t)$, *effectively relaxing the model's reliance on strict dynamics while maintaining strong stability guarantees. Simulation results further demonstrate that, even under stochastic disturbances, the state estimates converge and remain within a small neighborhood of the true values.*

Remark 3. *(Jazwinski (2007), Lemmas 7.1 and 7.2). With the LTV system* (8) *being UCO, the solution of* (26c) *is positive definite and uniformly bounded from above and below for all* $t \geq t_0$.

According to (6) and (25), define the estimation error

$$\tilde{\boldsymbol{x}}(t) \triangleq \boldsymbol{x}(t) - \hat{\boldsymbol{x}}(t). \tag{27}$$

Since the continuous-time LTV system (8) is UCO, it follows that $\tilde{\boldsymbol{x}}(t)$ is uniformly ultimately bounded Khalil (2002).

Remark 4. *An estimate of* $\mathbf{v}_L$ *is easily obtained from algebraic manipulations involving* (1) *and* (3b). *Notice that*

$$\hat{\mathbf{v}}_L(t) = \mathbf{v}_Q(t) - \ell\mathbf{S}(\hat{\mathbf{q}}(t))\hat{\boldsymbol{\omega}}(t) \quad \forall t \geq t_0, \tag{28}$$

where $\mathbf{v}_Q(t) \in \mathbb{R}^3$ *is the measured linear velocity of the UAV.*

Remark 5. *From a practical standpoint, balancing an inverted pendulum on a UAV implies that the aerial vehicle will predominantly be in a quasi-hover configuration, with the pendulum nearly always aligned vertically, i.e.,* $\mathbf{q} \approx [0\ 0\ -1]^\top$. *Consequently, according to (5b), the z-component of* $\mathbf{b}$ *will have minimal influence on the angular dynamics. This lack of excitation can lead to an observability issue, making accurate estimation of the z-component of* $\mathbf{b}$ *challenging. However, in typical indoor and outdoor aerial applications, this component is generally negligible. In scenarios where it is not, state augmentation can be employed to incorporate position and linear velocity, or alternatively, a scalar adaptive law can be specifically designed within the controller to compensate for external disturbances along the z-axis.*

5. KF-aided Controller Design

This section outlines the design of a nonlinear hierarchical tracking controller for the FIP system using the backstepping technique, ensuring close tracking of the desired trajectories. The estimated values from the proposed KF in Section 4.3 are integrated into the control framework to handle unmeasured states and unknown disturbances.

As discussed in Section 3.1, the underactuated nature of the FIP system prevents it from following arbitrary trajectories. Specifically, the thrust force $\mathbf{f}$ cannot generate acceleration in all directions during motion, and the UAV lacks the ability to apply torque directly to the inverted pendulum. To address this limitation, the trajectory tracking problem is reformulated as the generation of a vectored desired force. This force is designed to guide the load along a reference trajectory while simultaneously preventing the pendulum from toppling. It is decomposed into two components: one that regulates the position error and another that stabilizes the pendulum's orientation. To realize this desired force, a control law is developed for the UAV's angular velocity, enabling attitude adjustments that align the thrust direction with the required force vector.

5.1. Load Position Control

Begin by defining two reference tracking errors:

$$\mathbf{z_p} \triangleq \mathbf{p}_L - \mathbf{p}_{Ld} \in \mathbb{R}^3 \quad \text{and} \tag{29}$$

$$\mathbf{z_v} \triangleq \mathbf{v}_L - \dot{\mathbf{p}}_{Ld} \in \mathbb{R}^3, \tag{30}$$

whose derivatives, based on (3a) and (5a), follow as

$$\dot{\mathbf{z}}_\mathbf{p} = \mathbf{z_v}, \quad \text{and} \tag{31}$$

$$\dot{\mathbf{z}}_\mathbf{v} = \frac{1}{m_T}(\mathbf{f} + \mathbf{b})^\parallel - \frac{m_Q \ell}{m_T}\|\boldsymbol{\omega}\|^2 \mathbf{q} + g\mathbf{e}_3 - \ddot{\mathbf{p}}_{Ld}. \tag{32}$$

Let $\mathbf{f}_d \in \mathbb{R}^3$ represent the aforementioned vectored desired thrust force to be applied on the center of mass of the UAV. To stabilize the position error subsystem, define the component of $\mathbf{f}_d$ which is parallel to $\mathbf{q}$ as

$$\mathbf{f}_d^\parallel \triangleq -\hat{\boldsymbol{\xi}}^\parallel - \hat{\mathbf{b}}^\parallel + m_Q \ell \|\hat{\boldsymbol{\omega}}\|^2 \mathbf{q} \in \mathbb{R}^3, \tag{33}$$

where $\hat{\boldsymbol{\xi}} \in \mathbb{R}^3$ denotes the estimate of $\boldsymbol{\xi}$, which combines feedback and trajectory information, and is defined as

$$\boldsymbol{\xi} \triangleq m_T \left(\mathbf{K_p z_p} + \mathbf{K_v z_v} + g\mathbf{e}_3 - \ddot{\mathbf{p}}_{Ld}\right) \in \mathbb{R}^3, \tag{34}$$

where $\mathbf{K_p} \in \mathbb{R}^{3\times 3} \succ \mathbf{0}$ and $\mathbf{K_v} \in \mathbb{R}^{3\times 3} \succ \mathbf{0}$ are gain matrices. Since $\boldsymbol{\xi}$ in (34) depends on the unknown quantity $\mathbf{z_v}$, consider instead its estimated value $\hat{\mathbf{z}}_\mathbf{v} \triangleq \hat{\mathbf{v}}_L - \dot{\mathbf{p}}_{Ld} \in \mathbb{R}^3$ to construct $\hat{\boldsymbol{\xi}}$.

The first Lyapunov function candidate is put forward as

$$V_1 \triangleq \frac{1}{2}\mathbf{z_p}^\top \mathbf{K_p z_p} + \beta \mathbf{z_p}^\top \mathbf{z_v} + \frac{1}{2}\mathbf{z_v}^\top \mathbf{z_v}, \text{ with } \beta < \sqrt{\lambda_{\min}(\mathbf{K_p})}. \tag{35}$$

Based on (2), consider the decomposition $\boldsymbol{\xi} = \boldsymbol{\xi}^\parallel + \boldsymbol{\xi}^\perp$, and apply (31) and (32) to calculate the time derivative of V_1 as

$$\begin{aligned}\dot{V}_1 = &- W_1 + \frac{1}{m_T}\frac{\partial V_1}{\partial \mathbf{v}_L}^\top \boldsymbol{\xi}^\perp + \frac{1}{m_T}\frac{\partial V_1}{\partial \mathbf{v}_L}^\top \left(\mathbf{f}^\parallel + \boldsymbol{\xi}^\parallel + \mathbf{b}^\parallel\right.\\ &\left.- m_Q \ell \|\boldsymbol{\omega}\|^2 \mathbf{q}\right),\end{aligned} \tag{36}$$

where $\frac{\partial V_1}{\partial \mathbf{v}_L} = \beta \mathbf{z_p} + \mathbf{z_v} \in \mathbb{R}^3$, and

$$W_1 \triangleq \begin{bmatrix}\mathbf{z_p} & \mathbf{z_v}\end{bmatrix} \begin{bmatrix}\beta \mathbf{K_p} & \frac{\beta}{2}\mathbf{K_v} \\ \frac{\beta}{2}\mathbf{K_v} & -(\beta - \mathbf{K_v})\end{bmatrix} \begin{bmatrix}\mathbf{z_p} \\ \mathbf{z_v}\end{bmatrix} \in \mathbb{R}. \tag{37}$$

Note that W_1 is positive for any $\mathbf{z_p}, \mathbf{z_v} \neq \mathbf{0}$ if and only if

$$\beta < \min\left(\lambda_{\min}^{1/2}(\mathbf{K_p}), \lambda_{\min}(4\mathbf{K_p K_v}\left(4\mathbf{K_p} + \mathbf{K_v}^2\right)^{-1})\right). \tag{38}$$

According to (33), $\dot{V}_1$ in (36) can be rewritten as

$$\dot{V}_1 = -W_1 + \frac{1}{m_T}\frac{\partial V_1}{\partial \mathbf{v}_L}^\top \boldsymbol{\xi}^\perp + \Psi_1 + \frac{1}{m_T}\frac{\partial V_1}{\partial \mathbf{v}_L}^\top \left(\mathbf{f}^\parallel - \mathbf{f}_d^\parallel\right), \tag{39}$$

where $\Psi_1 \in \mathbb{R}$ is an auxiliary variable that includes error terms associated with (27), which arise due to the estimates considered in (33). This point is further elaborated in Appendix A.

5.2. Pendulum Direction Control

Define the desired pendulum direction as

$$\mathbf{q}_d \triangleq -\frac{\boldsymbol{\xi}}{\|\boldsymbol{\xi}\|} \in \mathbb{S}^2, \tag{40}$$

assuming that $\|\boldsymbol{\xi}\| > 0$. To align the inverted pendulum direction $\mathbf{q}$ with the desired direction $\mathbf{q}_d$, the pendulum direction error is set as

$$\mathbf{z_q} \triangleq \mathbf{q} - \mathbf{q}_d \in \mathbb{R}^3. \tag{41}$$

The second Lyapunov function candidate is thus designed as

$$V_2 \triangleq V_1 + \frac{h_\mathbf{q}}{2}\mathbf{z_q}^\top \mathbf{z_q}, \tag{42}$$

where $h_{\mathbf{q}} > 0$ is a matching parameter. The derivative of V_2, based on (3b) and (39), and for some $k_{\mathbf{q}} > 0$, gives

$$\begin{aligned}\dot{V}_2 = &-W_2 + \Lambda_1 + \Psi_1 + \frac{1}{m_T}\frac{\partial V_1}{\partial \mathbf{v}_L}^\top\left(\mathbf{f}^{\parallel} - \mathbf{f}_d^{\parallel}\right)\\ &+ h_{\mathbf{q}}\mathbf{q}_d^\top\left(\mathbf{S}(\mathbf{q})\boldsymbol{\omega} + \mathbf{S}(\mathbf{q})\mathbf{S}(\mathbf{q}_d)\frac{\dot{\boldsymbol{\xi}}}{\|\boldsymbol{\xi}\|} + \frac{k_{\mathbf{q}}}{h_{\mathbf{q}}}\mathbf{q}_d^{\perp}\right),\end{aligned} \tag{43}$$

where $W_2 \triangleq W_1 + k_{\mathbf{q}}\|\mathbf{z}_{\mathbf{q}}^{\perp}\|^2 > 0$ and where, for brevity, $\Lambda_1 \triangleq \frac{\|\xi\|}{m_T}\frac{\partial V_1}{\partial \mathbf{v}_L}\mathbf{z}_{\mathbf{q}}^{\perp} \in \mathbb{R}$.

To keep the notation concise, any function $\boldsymbol{\mu}$ with an explicit dependence on $\mathbf{v}_L$ will be represented in such a way that its time derivative can be expressed as

$$\dot{\boldsymbol{\mu}} = \dot{\boldsymbol{\mu}}|_{\mathbf{f}=\mathbf{f}_d^{\parallel}} + \frac{1}{m_T}\frac{\partial \boldsymbol{\mu}}{\partial \mathbf{v}_L}\left(\mathbf{f} - \mathbf{f}_d\right)^{\parallel}, \tag{44}$$

where $\dot{\boldsymbol{\mu}}|_{\mathbf{f}=\mathbf{f}_d^{\parallel}}$ is a term whose dependence on variable $\mathbf{f}$ is replaced by an explicit dependence on $\mathbf{f}_d^{\parallel}$, as given by (33). Furthermore, one can write a useful decomposition as

$$\dot{\boldsymbol{\mu}}|_{\mathbf{f}=\mathbf{f}_d^{\parallel}} = \widehat{\dot{\boldsymbol{\mu}}}|_{\mathbf{f}=\mathbf{f}_d^{\parallel}} + h(\widetilde{\mathbf{x}}), \tag{45}$$

with $\widehat{\dot{\boldsymbol{\mu}}}|_{\mathbf{f}=\mathbf{f}_d^{\parallel}}$ being a known term equivalent to calculating $\dot{\boldsymbol{\mu}}|_{\mathbf{f}=\mathbf{f}_d^{\parallel}}$ using the estimates $\widehat{\mathbf{v}}_L$, $\widehat{\boldsymbol{\omega}}$ and $\widehat{\mathbf{b}}$, while the remaining unknown terms, which are function of (27), are all gathered into $h(\widetilde{\mathbf{x}})$.

Next, define the inverted pendulum's angular velocity error as

$$\mathbf{z}_{\boldsymbol{\omega}} \triangleq \mathbf{S}(\mathbf{q})(\boldsymbol{\omega} - \boldsymbol{\omega}_d) \in \mathbb{R}^3, \tag{46}$$

where the desired inverted pendulum's angular velocity is designed as

$$\boldsymbol{\omega}_d \triangleq \frac{k_{\mathbf{q}}}{h_{\mathbf{q}}}\mathbf{S}(\mathbf{q})\mathbf{q}_d - \frac{1}{\|\xi\|}\mathbf{S}(\mathbf{q}_d)\widehat{\dot{\boldsymbol{\xi}}}|_{\mathbf{f}=\mathbf{f}_d^{\parallel}} \in \mathbb{R}^3. \tag{47}$$

The third Lyapunov function is then constructed as

$$V_3 \triangleq V_2 + \frac{h_{\boldsymbol{\omega}}}{2}\mathbf{z}_{\boldsymbol{\omega}}^\top\mathbf{z}_{\boldsymbol{\omega}}, \tag{48}$$

where $h_{\boldsymbol{\omega}} > 0$ is a matching parameter. Using (5b), and for some $k_{\boldsymbol{\omega}} > 0$, compute the time derivative of V_3 as

$$\begin{aligned}\dot{V}_3 = &-W_3 + \Lambda_1 + \Psi_2 + \boldsymbol{\delta}^\top(\mathbf{f}^{\parallel} - \mathbf{f}_d^{\parallel})^{\parallel} + h_{\boldsymbol{\omega}}\mathbf{z}_{\boldsymbol{\omega}}^\top\left(\frac{1}{m_Q\ell}\mathbf{f}^{\perp}\right.\\ &\left.+\dot{\mathbf{z}}_{\omega}|_{\mathbf{f}=\mathbf{f}_d^{\parallel}} + \frac{h_{\mathbf{q}}}{h_{\boldsymbol{\omega}}}\mathbf{q}_d + \frac{k_{\boldsymbol{\omega}}}{h_{\boldsymbol{\omega}}}\mathbf{z}_{\boldsymbol{\omega}} + \frac{1}{m_Q\ell}\mathbf{b}\right),\end{aligned} \tag{49}$$

where $W_3 \triangleq W_2 + k_{\boldsymbol{\omega}}\mathbf{z}_{\boldsymbol{\omega}}^\top\mathbf{z}_{\boldsymbol{\omega}} > 0$, and where

$$\boldsymbol{\delta} \triangleq \frac{1}{m_T}\frac{\partial V_1}{\partial \mathbf{v}_L}^\top - \frac{h_{\mathbf{q}}}{\|\xi\|}\frac{\partial \xi}{\partial \mathbf{v}_L}^\top\mathbf{S}^2(\widehat{\mathbf{q}_d})\mathbf{q} + h_{\boldsymbol{\omega}}\left.\frac{\partial \mathbf{z}_{\boldsymbol{\omega}}}{\partial \mathbf{v}_L}\right|_{\text{est}}^\top\mathbf{z}_{\boldsymbol{\omega}} \in \mathbb{R}^3 \tag{50}$$

is introduced to simplify expressions. Note that $\widehat{\mathbf{q}_d}$ and $\left.\frac{\partial \mathbf{z}_{\boldsymbol{\omega}}}{\partial \mathbf{v}_L}\right|_{\text{est}}$ are pseudo-estimates of $\mathbf{q}_d$ and $\frac{\partial \mathbf{z}_{\boldsymbol{\omega}}}{\partial \mathbf{v}_L}$, respectively.

In view of (49), and by following an approach similar to the one leading to $\mathbf{f}_d^{\parallel}$, the desired force's orthogonal component $\mathbf{f}_d^{\perp} \in \mathbb{R}^3$ is now defined as:

$$\mathbf{f}_d^{\perp} \triangleq -m_Q\ell\left(\widehat{\dot{\mathbf{z}}_{\omega}}|_{\mathbf{f}=\mathbf{f}_d^{\parallel}} + \frac{h_{\mathbf{q}}}{h_{\boldsymbol{\omega}}}\widehat{\mathbf{q}_d} + \frac{k_{\boldsymbol{\omega}}}{h_{\boldsymbol{\omega}}}\widehat{\mathbf{z}_{\boldsymbol{\omega}}} + \frac{1}{m_Q\ell}\widehat{\mathbf{b}}\right)^{\perp}. \tag{51}$$

Therefore, based on (33) and (51), rewrite (49) as

$$\dot{V}_3 = -W_3 + \Lambda_1 + \Psi_3 + \left(\boldsymbol{\delta}^\top\mathbf{q}\mathbf{q}^\top - \frac{h_{\boldsymbol{\omega}}}{m_Q\ell}\mathbf{z}_{\boldsymbol{\omega}}^\top\mathbf{S}^2(\mathbf{q})\right)(\mathbf{f} - \mathbf{f}_d), \tag{52}$$

where the complete desired thrust force is formulated as

$$\mathbf{f}_d \triangleq \mathbf{f}_d^{\parallel} + \mathbf{f}_d^{\perp}. \tag{53}$$

Hence, the magnitude of the desired net thrust is set as $T_d \triangleq \|\mathbf{f}_d\|$. This force is applied along the desired direction of $-\mathbf{r}_{3d} \triangleq \frac{1}{T_d}\mathbf{f}_d \in \mathbb{S}^2$. However, the underactuated UAV's effective thrust can only be generated along $-\mathbf{r}_3$. As a result, the thrust control law is set as

$$T \triangleq T_d\mathbf{r}_{3d}^\top\mathbf{r}_3. \tag{54}$$

5.3. Nonlinear UAV Attitude Control

The objective of this subsection is to design the control law for the UAV's angular velocity to align $\mathbf{r}_3$ with $\mathbf{r}_{3d}$. To achieve this, introduce a new system error defined as

$$\mathbf{z}_{\mathbf{r}} \triangleq \mathbf{r}_3 - \mathbf{r}_{3d} \in \mathbb{R}^3. \tag{55}$$

Set the angular velocity control law as

$$\begin{aligned}\boldsymbol{\Omega} \triangleq -\mathbf{S}^2(\mathbf{e}_3)&\left(\mathbf{R}^\top\mathbf{S}(\mathbf{r}_{3d})\widehat{\dot{\mathbf{r}}_{3d}} + \frac{k_{\mathbf{r}}}{h_{\mathbf{r}}}\mathbf{S}(\mathbf{e}_3)\mathbf{R}^\top\mathbf{r}_{3d}\right.\\ &\left.+\frac{T_d}{h_{\mathbf{r}}m_T}\mathbf{S}(\mathbf{e}_3)\mathbf{R}^\top\widehat{\boldsymbol{\delta}}^{\parallel} + \frac{h_{\boldsymbol{\omega}}}{h_{\mathbf{r}}}\frac{T_d}{m_Q\ell}\mathbf{S}(\mathbf{e}_3)\mathbf{R}^\top\widehat{\mathbf{z}_{\boldsymbol{\omega}}}\right) - \gamma\mathbf{e}_3,\end{aligned} \tag{56}$$

where $\gamma \in \mathbb{R}$ denotes the third component of $\boldsymbol{\Omega}$, and $k_{\mathbf{r}} > 0$ is a feedback control gain. Note that γ is independent of the trajectory tracking objective and can be designed arbitrarily, provided that it is bounded. Additionally, $\widehat{\dot{\mathbf{r}}_{3d}}$ and $\widehat{\boldsymbol{\delta}}$ are pseudo-estimates of $\dot{\mathbf{r}}_{3d}$ and $\boldsymbol{\delta}$.

Considering the error $\mathbf{z}_{\mathbf{r}}$, set the fourth Lyapunov function as

$$V_4 \triangleq V_3 + \frac{h_{\mathbf{r}}}{2}\mathbf{z}_{\mathbf{r}}^\top\mathbf{z}_{\mathbf{r}}, \tag{57}$$

for $h_{\mathbf{r}} > 0$. Consequently, in view of (52) and (56), and $\mathbf{f} = \mathbf{r}_3\mathbf{r}_3^\top\mathbf{f}_d$, compute the time derivative of V_4 as

$$\dot{V}_4 = -W_4 + \Lambda_1 + \Psi_4, \tag{58}$$

where $W_4 \triangleq W_3 + k_{\mathbf{r}}\|\mathbf{S}^2(\mathbf{r}_3)\mathbf{z}_{\mathbf{r}}\|^2 > 0$.

6. Stability Analysis

To analyze the stability of the entire FIP system, express the Lyapunov function defined in (57) in concise vector notation as

$$V_4 = \mathbf{z}^\top \mathbf{Q}\mathbf{z}, \tag{59}$$

where

$$\mathbf{z} \triangleq \begin{bmatrix} \mathbf{z}_\mathbf{p}^\top & \mathbf{z}_\mathbf{v}^\top & \mathbf{z}_\mathbf{q}^\top & \mathbf{z}_\omega^\top & \mathbf{z}_\mathbf{r}^\top \end{bmatrix}^\top \in \mathbb{R}^{15}, \tag{60}$$

and $\mathbf{Q} \in \mathbb{R}^{15\times 15}$ is a positive definite matrix defined by

$$\mathbf{Q} \triangleq \frac{1}{2}\,\mathrm{blkdiag}\left(\begin{bmatrix} \mathbf{K_p} & \beta\mathbf{I} \\ \beta\mathbf{I} & \mathbf{I} \end{bmatrix}, h_\mathbf{q}\mathbf{I}, h_\omega \mathbf{I}, h_\mathbf{r}\mathbf{I} \right), \tag{61}$$

for

$$0 < \beta < \sqrt{\lambda_{\min}(\mathbf{K_p})}. \tag{62}$$

It follows then from (58) that

$$\dot{V}_4 = -(\mathbf{P}\mathbf{z})^\top \mathbf{J}(\mathbf{P}\mathbf{z}) + \Psi_4, \tag{63}$$

where $\mathbf{P} \triangleq \mathrm{diag}(\mathbf{I}, \mathbf{I}, -\mathbf{S}^2(\mathbf{q}), \mathbf{I}, -\mathbf{S}^2(\mathbf{r}_3)) \in \mathbb{R}^{15\times 15}$ and $\mathbf{J} \in \mathbb{R}^{15\times 15}$ is defined as

$$\mathbf{J} \triangleq \begin{bmatrix} \beta\mathbf{K_p} & \frac{\beta}{2}\mathbf{K_v} & -\frac{\beta\|\xi\|}{2m_T}\mathbf{I} & \mathbf{0} & \mathbf{0} \\ \frac{\beta}{2}\mathbf{K_v} & -(\beta\mathbf{I} - \mathbf{K_v}) & -\frac{\|\xi\|}{2m_T}\mathbf{I} & \mathbf{0} & \mathbf{0} \\ -\frac{\beta\|\xi\|}{2m_T}\mathbf{I} & -\frac{\|\xi\|}{2m_T}\mathbf{I} & k_\mathbf{q}\mathbf{I} & \mathbf{0} & \mathbf{0} \\ \mathbf{0} & \mathbf{0} & \mathbf{0} & k_\omega\mathbf{I} & \mathbf{0} \\ \mathbf{0} & \mathbf{0} & \mathbf{0} & \mathbf{0} & k_\mathbf{r}\mathbf{I} \end{bmatrix}, \tag{64}$$

which is positive definite provided that β satisfies (38), and

$$\frac{k_\mathbf{q}}{\bar{\xi}} > \lambda_{\max}\left((\mathbf{K_p} - \beta^2\mathbf{I})(4\mathbf{K_p}\mathbf{K_v} - \beta\mathbf{K_v}^2 - 4\beta\mathbf{K_p})^{-1} \right), \tag{65}$$

where $\bar{\xi} > 0$ is such that $\|\xi(t)\| < \bar{\xi}$ for all $t \geq t_0$.

Theorem 2. *Consider the FIP system described by* (3) *and* (5) *operating in closed-loop using* (54) *and* (56)*, alongside the KF formulated in* (26)*. For any positive control gains satisfying* (38) *and* (65)*, the closed-loop system errors are uniformly ultimately bounded (UUB), i.e., the tracking error* $\mathbf{z}$ *in* (60) *and the estimation error* $\tilde{\mathbf{x}}$ *in* (27) *are UUB.*

Proof. According to Proposition 1 in Lee (2017), it must be

$$\frac{\|w(\mathbf{q}, \mathbf{q}_d)\|^2}{2} \leq f(\mathbf{z_q}) \leq \frac{\|w(\mathbf{q}, \mathbf{q}_d)\|^2}{2 - \gamma_q}, \text{ if } f(\mathbf{z_q}) \leq \gamma_q < 2,$$

where $f(\mathbf{z_q}) \triangleq 0.5\mathbf{z}_\mathbf{q}^\top \mathbf{z_q}$ and $w(\mathbf{q}, \mathbf{q}_d) \triangleq \mathbf{S}(\mathbf{q}_d)\mathbf{q}$, and

$$\frac{\|w(\mathbf{r}_3, \mathbf{r}_{3d})\|^2}{2} \leq f(\mathbf{z_r}) \leq \frac{\|w(\mathbf{r}_3, \mathbf{r}_{3d})\|^2}{2 - \gamma_r}, \text{ if } f(\mathbf{z_r}) \leq \gamma_r < 2,$$

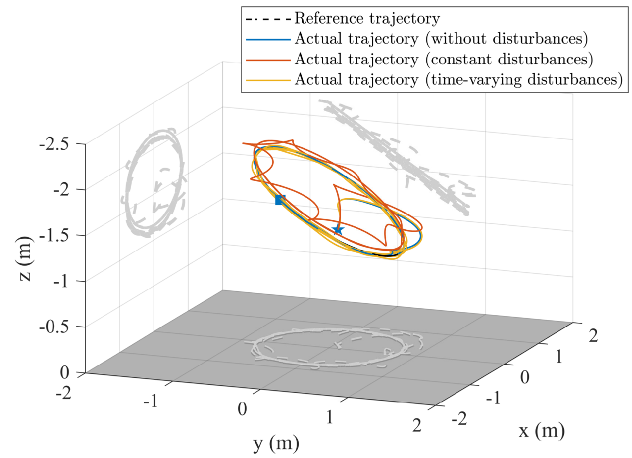

Figure 1: Simulation. Reference trajectory $\mathbf{p}_{Ld}$ versus actual load position $\mathbf{p}_L$. Start and end locations are marked with a star and square, respectively.

where $f(\mathbf{z_r}) \triangleq \frac{1}{2}\mathbf{z}_\mathbf{r}^\top \mathbf{z_r}$ and $w(\mathbf{r}_3, \mathbf{r}_{3d}) \triangleq \mathbf{S}(\mathbf{r}_{3d})\mathbf{r}_3$. Therefore, note that V_4 in (59) obeys to

$$(\mathbf{P}\mathbf{z})^\top \mathbf{Q}(\mathbf{P}\mathbf{z}) \leq V_4 \leq (\mathbf{P}\mathbf{z})^\top \overline{\mathbf{Q}}(\mathbf{P}\mathbf{z}), \tag{66}$$

where $\overline{\mathbf{Q}} \triangleq (\mathrm{diag}(1, 1, \frac{2}{2-\gamma_q}, 1, \frac{2}{2-\gamma_r}) \otimes \mathbf{I})\mathbf{Q}$. Using Young's inequality, $\dot{V}_4$ in (63) can be rewritten as

$$\dot{V}_4 = -(\mathbf{P}\mathbf{z})^\top \mathbf{J}\overline{\mathbf{Q}}^{-1}\overline{\mathbf{Q}}(\mathbf{P}\mathbf{z}) + \Psi_4 \leq -\frac{\lambda_{\min}(\mathbf{J}^\star)}{\lambda_{\max}(\overline{\mathbf{Q}})} V_4 + \delta_{V_4}, \tag{67}$$

where $\delta_{V_4} > 0$ is a finite constant (cf. Appendix B). Hence, the closed-loop system error $\mathbf{z}$ ultimately converges to the set defined by $\Xi_\mathbf{z} \triangleq \left\{ \|\mathbf{z}\| \leq \sqrt{\frac{\delta_{V_4}\lambda_{\max}(\overline{\mathbf{Q}})}{\lambda_{\min}(\mathbf{J}^\star)\lambda_{\min}(\mathbf{Q})}} \right\}$. □

7. Simulation Results

The controller was realized and validated in a MATLAB/Simulink environment. Consider a FIP system with $m_Q = 0.26$ kg, $m_L = 0.03$ kg, $g = 9.81$ m/s^2 and $\ell = 0.7$ m. The reference trajectory is selected as

$$\mathbf{p}_{Ld}(\vartheta) \triangleq \begin{bmatrix} 0.8\sin\left(\vartheta(t) + \frac{\pi}{2}\right) \\ 0.8\sin(\vartheta(t)) \\ 0.5\sin(\vartheta(t)) - 1.6 \end{bmatrix} \text{(m)}, \tag{68}$$

where $\vartheta(t)$ is a pseudo velocity parameter defined as

$$\vartheta(t) \triangleq 0.5 \int_{t_0}^{t} \left\| \frac{\partial \mathbf{p}_{Ld}(\vartheta(t))}{\partial \vartheta(t)} \right\|^{-1} d\tau, \tag{69}$$

meaning that $\|\dot{\mathbf{p}}_{Ld}(t)\| = 0.5$ m/s for all $t \geq t_0$.

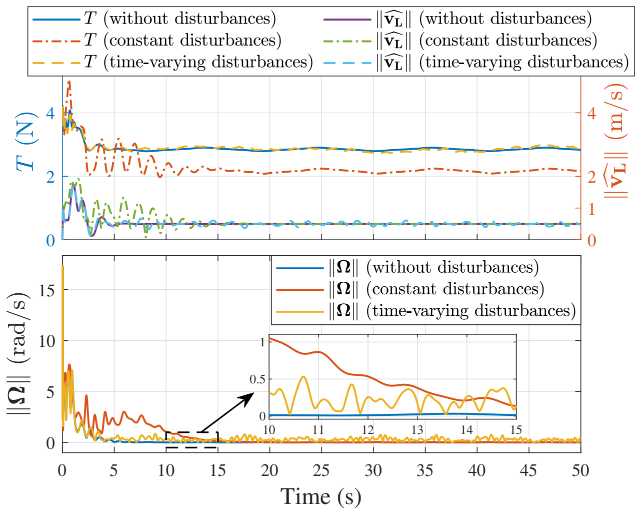

Figure 2: Simulation. Top: thrust and evolution of estimated load linear speed. Bottom: norm of angular velocity command.

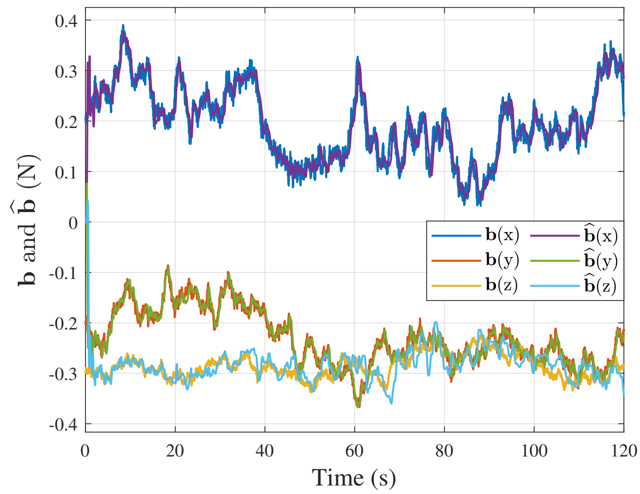

Figure 4: Simulation. Evolution of actual stochastic perturbations $\mathbf{b}$ (derived from white Gaussian noise using (71)) versus estimated disturbances $\widehat{\mathbf{b}}$. The initial value of $\widehat{\mathbf{b}}(0)$ is zero.

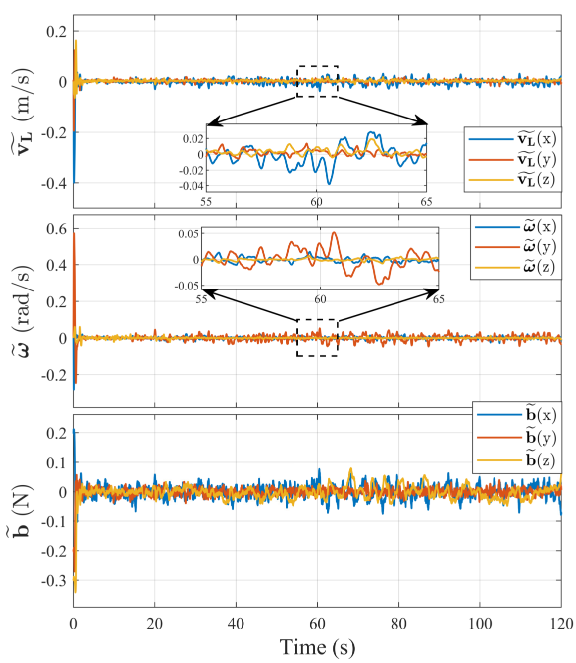

Figure 3: Simulation. Evolution of the estimation errors under stochastic disturbances.

The initial load position and direction of the inverted pendulum were set as

$$\mathbf{p}_L(t_0) \triangleq [0\ \ 0.2\ \ -0.3]^\mathsf{T}(\mathrm{m}) \ \text{ and}$$
$$\mathbf{q}(t_0) \triangleq \left[\frac{\sin(5^\circ)}{\sqrt{2}}\ \frac{\sin(5^\circ)}{\sqrt{2}}\ -\cos(5^\circ)\right]^\mathsf{T}. \tag{70}$$

The linear and angular velocities were initially set to zero. The initial state estimation $\hat{\mathbf{x}}(t_0)$ was set as $\left[\mathbf{e}_3^\mathsf{T}\ \mathbf{0}\ \mathbf{0}\right]^\mathsf{T}$, thus causing deliberately large initial estimation errors intended to validate the effectiveness of the proposed strategy. The UAV's initial attitude was aligned with $\{I\}$, i.e., $\mathbf{R}(0) \triangleq \mathbf{I}$.

The controller gains employed in the simulation are: $\mathbf{K_p} = 12\mathbf{I}$, $\mathbf{K_v} = 1.5\mathbf{I}$, $\beta = 0.3$, $k_\mathbf{q} = 20$, $k_\omega = 3$, $k_\mathbf{r} = 120$, $h_\mathbf{q} = 10$, $h_\omega = 1.3$ and $h_\mathbf{r} = 30$. The KF parameters are chosen as $\mathcal{Q} = \mathrm{diag}(10^{-7}\mathbf{I},\ 10^{-4}\mathbf{I},\ \mathrm{diag}(10\ 10\ 0.1))$, $\mathcal{R} = 3 \times 10^{-5}\mathbf{I}$, $\mathcal{P}(t_0) = \mathrm{diag}(10^{-4}\mathbf{I},\ \mathbf{I},\ \mathbf{I})$.

The disturbances used to test the proposed method in simulation are categorized into three cases:

(i) *none*, i.e., $\mathbf{b} = \mathbf{0}$;

(ii) *constant*, with $\mathbf{b} = [-0.5\ 0.5\ \ -0.8]^\mathsf{T}$;

(iii) *stochastic*, characterized by random perturbations governed by

$$\dot{\mathbf{b}} \triangleq 1.5\,\mathrm{diag}(13\ 15\ 22)^{-1}\left[-\mathbf{b} + 5\,\mathrm{diag}(6.5\ 5\ 4)\mathbf{w_d}\right], \tag{71}$$

where $\mathbf{w_d} \in \mathbb{R}^3$ is a vector of zero-mean white Gaussian noise sequences generated from different seeds, with standard deviation set to 0.1. The initial value of $\mathbf{b}$ was set to $[0.2\ \ -0.2\ \ -0.3]^\mathsf{T}$ (cf. Fig. 4).

The reference and actual trajectories, as described by the FIP, are illustrated in Fig. 1 for three disturbance scenarios. In Fig. 2, the evolution of control inputs T and $\mathbf{\Omega}$ is depicted. The presence of a constant lifting disturbance along the z-axis reduces the vehicle's thrust, simulating a lighter UAV. Notably, the estimated load linear speed remains close to the reference trajectory speed of 0.5 m/s. The evolution of all estimation errors under time-varying disturbances is shown in Fig. 3. For completeness, Fig. 4 shows the evolution of the actual stochastic disturbances alongside the corresponding estimates.

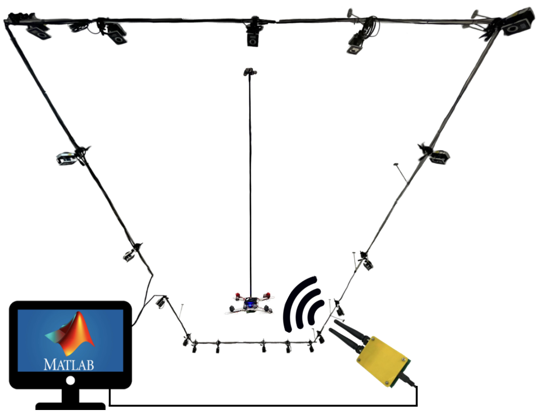

Figure 5: Experimental setup. The FIP is tracked using VICON Vantage motion capture cameras. Actuation signals are computed in MATLAB and transmitted via RF transmitter to the UAV's main control board for execution.

8. Experimental Results

8.1. Setup

The test arena at the SCORE laboratory of the University of Macau features a MATLAB/Simulink environment that seamlessly integrates sensors, control algorithms, and communications with the UAV. In the experiment, a quadrotor vehicle acts as the actuator for the FIP system. The inverted pendulum consists of a 1-meter carbon fiber rod with reflective marks attached to its tip.

The experimental setup, including the FIP prototype, is shown in Fig. 5. In this setup, a VICON motion capture system is employed to measure the position of the quadrotor and the suspended load, and measure the vehicle's attitude. Control command signals are transmitted to the quadrotor via an RF link at a frequency of 45 Hz.

The masses used for experiments are $m_Q = 0.253$ kg and $m_L = 0.032$ kg. The controller parameters were adjusted as $\mathbf{K_p} = 9\mathbf{I}$, $\mathbf{K_v} = 2.3\mathbf{I}$, $\beta = 0.2$, $k_\mathbf{q} = 24.6$, $k_\omega = 6$, $k_\mathbf{r} = 550$, $h_\mathbf{q} = 12$, $h_\omega = 1.95$ and $h_\mathbf{r} = 100$. The KF parameters were chosen as $\mathcal{Q} = \mathrm{diag}(10^{-7}\mathbf{I},\ 10^{-4}\mathbf{I},\ \mathrm{diag}(40, 40, 10^{-5}))$, $\mathcal{R} = 10^{-5}\mathbf{I}$, $\mathcal{P}(t_0) = \mathrm{diag}(10^{-4}\mathbf{I},\ \mathbf{I},\ \mathbf{I})$.

8.2. Trajectory Tracking

In the FIP trajectory tracking experiment, the reference trajectory evolves as described in (68). The results of this experiment are presented in Fig. 6. The norm of the estimated load's linear velocity, denoted by $\|\hat{\mathbf{v}}_L\|$, starts at zero and stabilizes at a steady-state mean value of 0.51 m/s. The presence of oscillations is attributed to the sensitive dynamics of the underactuated FIP system.

It is noteworthy that $\|\mathbf{z_p}\|$ takes approximately 5 seconds to achieve steady-state behavior, with a mean value of 9.72 cm, which is satisfactory for this application. Finally, it is important to emphasize that the command signals, T and $\mathbf{\Omega}$, remain within reasonable and expected ranges.

It is also important to emphasize that, although not addressed theoretically due to the inherent challenges in modeling time-varying disturbances, the disturbance term $\mathbf{b}$ can, in practice, loosely capture certain effects associated with internal model parametric uncertainty. While constant disturbances may not fully reflect realistic conditions, since constant parametric uncertainty within the internal model does not necessarily translate to a constant disturbance in the inertial (non-rotating) frame, this practical flexibility allows $\mathbf{b}$ to absorb some of these effects to a useful extent. Indeed, these effects are likely on display in Fig. 6, as the tests were conducted indoors, meaning there was no wind or other external influences on the dynamics of the FIP system.

In Hehn and D'Andrea (2011), the authors employed a linearized model that restricts their method to operate effectively only around the operating point. In contrast, our proposed approach features a significantly broader operating range, achieving better tracking performance even with substantial initial deviations. Furthermore, due to a carefully designed adaptive nonlinear backstepping controller that accounts for pendulum attitude error, our method ensures the FIP system remains upright and consistent with an extended reference state throughout the trajectory tracking process.

9. Conclusion

This paper addressed the trajectory tracking problem for an underactuated flying inverted pendulum, operating without direct measurements of its linear and angular velocities and under the influence of unknown constant perturbations. To estimate the unmeasured state variables, a Kalman filter was implemented based on a uniformly completely observable linear time-varying system that captures the pendulum's angular dynamics. Theoretical analysis of the proposed nonlinear backstepping controller confirmed that all errors in the closed-loop system are uniformly ultimately bounded. The effectiveness and robustness of the proposed methodology were further validated through both simulation and experimental results.

CRediT authorship contribution statement

Weiming Yang: Conceptualization, Methodology, Investigation, Writing – original draft. **Joel Reis**: Investigation, Visualization, Writing – review & editing. **Gan Yu**: Visualization, Writing – review & editing. **Carlos Silvestre**: Funding acquisition, Supervision, Writing – review & editing.

Declaration of competing interest

The authors declare that they have no known competing financial interests or personal relationships that could have appeared to influence the work reported in this paper.

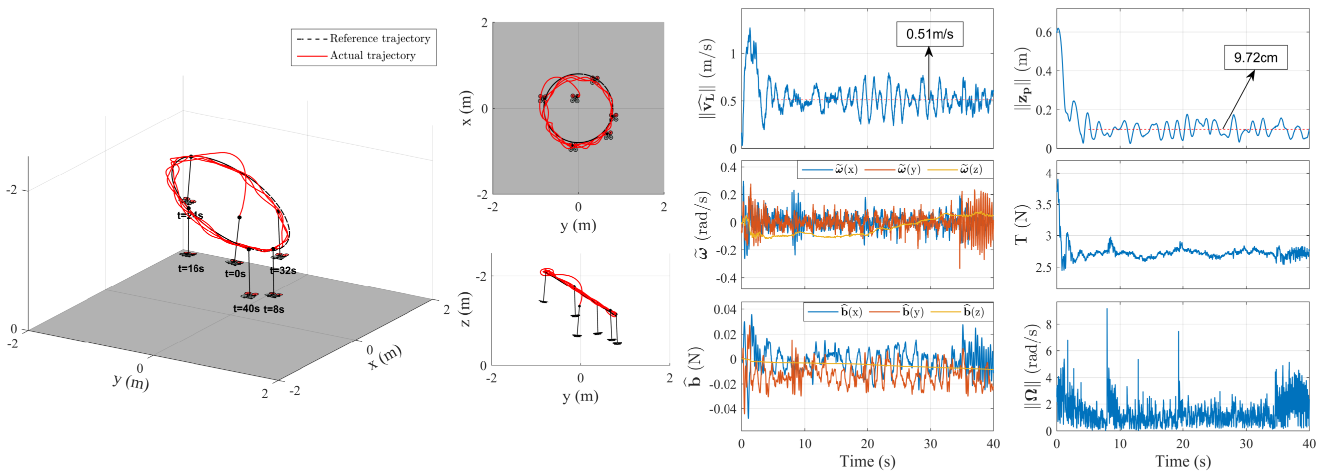

Figure 6: Experiment. *Left column*: actual trajectory versus reference trajectory, with specific instances of the maneuver timestamped for reference. *Middle left column*: two planar perspectives. *Middle right column*: evolution of $\|\widehat{\mathbf{v}}_L\|$, $\widetilde{\boldsymbol{\omega}}$ and $\widehat{\mathbf{b}}$. *Right column*: evolution $\|\mathbf{z}_\mathbf{p}\|$, T and $\|\boldsymbol{\Omega}\|$.

Appendix A Auxiliary computations

The auxiliary variables Ψ_1 in (39), Ψ_2 in (49), Ψ_3 in (52) and Ψ_4 in (58) are computed as follows:

$$\Psi_1 \triangleq \frac{1}{m_T}\frac{\partial V_1}{\partial \mathbf{v}_L}^{\top}\left(\widetilde{\mathbf{b}}^{\parallel} + m_Q\ell(\|\widehat{\boldsymbol{\omega}}\|^2 - \|\boldsymbol{\omega}\|^2)\mathbf{q} + \mathbf{K}_\mathbf{v}{}^{\parallel}\widetilde{\mathbf{v}}_L\right), \tag{72}$$

$$\Psi_2 \triangleq \Psi_1 - \frac{h_\mathbf{q}}{\|\xi\|}\mathbf{q}^\top\mathbf{S}^2(\mathbf{q}_d)\frac{\partial \xi}{\partial \mathbf{v}_L}\left(\widetilde{\mathbf{b}}^{\parallel} + m_Q\ell(\|\widehat{\boldsymbol{\omega}}\|^2 - \|\boldsymbol{\omega}\|^2)\mathbf{q}\right), \tag{73}$$

$$\Psi_3 \triangleq \Psi_2 + h_\omega \mathbf{z}_\omega^\top\left((\dot{\mathbf{z}}_\omega|_{\mathbf{f}=\mathbf{f}_d^\parallel} - \widehat{\dot{\mathbf{z}}_\omega}|_{\mathbf{f}=\mathbf{f}_d^\parallel}) + \frac{h_\mathbf{q}}{h_\omega}(\mathbf{q}_d - \widehat{\mathbf{q}_d}) + \frac{k_\omega}{h_\omega}(\mathbf{z}_\omega - \widehat{\mathbf{z}_\omega}) + \frac{1}{m_Q\ell}\widetilde{\mathbf{b}}\right), \text{ and} \tag{74}$$

$$\Psi_4 \triangleq \Psi_3 + h_\mathbf{r}\mathbf{r}_{3d}^\top\mathbf{R}\mathbf{S}(\mathbf{e}_3)\left(-\mathbf{R}^\top\mathbf{S}(\mathbf{r}_{3d})(\dot{\mathbf{r}}_{3d} - \widehat{\dot{\mathbf{r}}_{3d}}) - \frac{T_d}{h_\mathbf{r}m_T}\mathbf{S}(\mathbf{e}_3)\mathbf{R}^\top(\delta - \widehat{\delta})^\parallel - \frac{h_\omega}{h_\mathbf{r}}\frac{T_d}{m_Q\ell}\mathbf{S}(\mathbf{e}_3)\mathbf{R}^\top(\mathbf{z}_\omega - \widehat{\mathbf{z}_\omega})\right). \tag{75}$$

Appendix B Boundedness of δ_{V_4}

Using Young's inequality, Ψ_1 can be expressed as

$$\Psi_1 \leq \frac{\gamma_1}{2}\beta^2\|\mathbf{z}_\mathbf{p}\|^2 + \frac{\gamma_1}{2}\|\mathbf{z}_\mathbf{v}\|^2 + \frac{1}{2\gamma_1}\delta_{\Psi_1}, \tag{76}$$

where $\gamma_1 \in \mathbb{R}_{>0}$ and $\delta_{\Psi_1} \triangleq \|\widetilde{\mathbf{b}}^\parallel + m_Q\ell(\|\widehat{\boldsymbol{\omega}}\|^2 - \|\boldsymbol{\omega}\|^2)\mathbf{q} + \mathbf{K}_\mathbf{v}\mathbf{q}\mathbf{q}^\top\widetilde{\mathbf{v}}_L\|^2$. On account of the boundedness of $\widetilde{\boldsymbol{x}}$, it follows that $\widetilde{\mathbf{v}}_L$, $\widetilde{\boldsymbol{\omega}}$ and $\widetilde{\mathbf{b}}$ are bounded. Therefore, δ_{Ψ_1} is also bounded. Then, using Young's inequality again to Ψ_2, one has

$$\Psi_2 \leq \Psi_1 + \frac{\gamma_2}{2}\frac{h_\mathbf{q}}{\|\xi\|}\|\mathbf{q}^\top\mathbf{S}^2(\mathbf{q}_d)\|^2 + \frac{1}{2\gamma_2}\delta_{\Psi_2}, \tag{77}$$

where $\gamma_2 \in \mathbb{R}_{>0}$ and $\delta_{\Psi_2} \triangleq \|\mathbf{K}_\mathbf{v}\widetilde{\mathbf{b}}^\parallel + m_Q\ell(\|\widehat{\boldsymbol{\omega}}\|^2 - \|\boldsymbol{\omega}\|^2)\mathbf{q}\|^2$. Since $\widetilde{\boldsymbol{\omega}}$ and $\widetilde{\mathbf{b}}$ are bounded, δ_{Ψ_2} is also bounded. Applying Young's inequality to Ψ_3, it follows that

$$\Psi_3 \leq \Psi_2 + \frac{\gamma_3}{2}\|\mathbf{z}_\omega\|^2 + \frac{1}{2\gamma_3}\delta_{\Psi_3}, \tag{78}$$

where $\gamma_3 \in \mathbb{R}_{>0}$ and $\delta_{\Psi_3} \triangleq \|\dot{\mathbf{z}}_\omega|_{\mathbf{f}=\mathbf{f}_d^\parallel} - \widehat{\dot{\mathbf{z}}_\omega}|_{\mathbf{f}=\mathbf{f}_d^\parallel} + \frac{h_\mathbf{q}}{h_\omega}(\mathbf{q}_d - \widehat{\mathbf{q}_d}) + \frac{k_\omega}{h_\omega}(\mathbf{z}_\omega - \widehat{\mathbf{z}_\omega}) + \frac{1}{m_Q\ell}\widetilde{\mathbf{b}}\|^2$. Since $\widetilde{\mathbf{v}}_L$ is bounded, then $\xi - \widehat{\xi}$ and $\mathbf{q}_d - \widehat{\mathbf{q}_d}$ are bounded. Moreover, on account of $\widetilde{\boldsymbol{x}}$ being bounded, $\dot{\mathbf{z}}_\omega|_{\mathbf{f}=\mathbf{f}_d^\parallel} - \widehat{\dot{\mathbf{z}}_\omega}|_{\mathbf{f}=\mathbf{f}_d^\parallel}$ and $\mathbf{z}_\omega - \widehat{\mathbf{z}_\omega}$ are also bounded. Hence, δ_{Ψ_3} is bounded. Likewise, $\dot{\mathbf{r}}_{3d} - \widehat{\dot{\mathbf{r}}_{3d}}$ and $\boldsymbol{\delta} - \widehat{\boldsymbol{\delta}}$ are also bounded. Due to the norm-preserving property of $\mathbf{R}$, and since $\mathbf{r}_3$ and $\mathbf{r}_{3d}$ are unit vectors, $\delta_{\Psi_4} \triangleq h_\mathbf{r}\mathbf{r}_{3d}^\top\mathbf{R}\mathbf{S}(\mathbf{e}_3)(-\mathbf{R}^\top\mathbf{S}(\mathbf{r}_{3d})(\dot{\mathbf{r}}_{3d} - \widehat{\dot{\mathbf{r}}_{3d}}) - \frac{T_d}{h_\mathbf{r}m_T}\mathbf{S}(\mathbf{e}_3)\mathbf{R}^\top(\delta - \widehat{\delta})^\parallel - \frac{h_\omega}{h_\mathbf{r}}\frac{T_d}{m_Q\ell}\mathbf{S}(\mathbf{e}_3)\mathbf{R}^\top(\mathbf{z}_\omega - \widehat{\mathbf{z}_\omega}))$ is bounded as well. In turn, the boundedness of δ_{V_4} in (67) is established, where $\delta_{V_4} \triangleq \delta_{\Psi_1} + \delta_{\Psi_2} + \delta_{\Psi_3} + \delta_{\Psi_4}$.

Then $\dot{V}_4$ in (63) can be expressed as

$$\dot{V}_4 = -(\mathbf{P}\mathbf{z})^\top\mathbf{J}\overline{\mathbf{Q}}^{-1}\overline{\mathbf{Q}}(\mathbf{P}\mathbf{z}) + \Psi_4 \leq -(\mathbf{P}\mathbf{z})^\top\mathbf{J}^\star\overline{\mathbf{Q}}^{-1}\overline{\mathbf{Q}}(\mathbf{P}\mathbf{z}) + \delta_{V_4}$$
$$\leq -\frac{\lambda_{\min}(\mathbf{J}^\star)}{\lambda_{\max}(\overline{\mathbf{Q}})}V_4 + \delta_{V_4},$$

$$\tag{79}$$

where

$$\mathbf{J}^\star \triangleq \mathbf{J} + \begin{bmatrix} -\frac{\gamma_1}{2}\beta^2\mathbf{I} & -\frac{\gamma_1}{4}\mathbf{I} & \mathbf{0} & \mathbf{0} & \mathbf{0} \\ -\frac{\gamma_1}{4}\mathbf{I} & \mathbf{0} & \mathbf{0} & \mathbf{0} & \mathbf{0} \\ \mathbf{0} & \mathbf{0} & -\frac{\gamma_2}{2}\frac{h_{\mathbf{q}}}{\|\xi\|}\mathbf{I} & \mathbf{0} & \mathbf{0} \\ \mathbf{0} & \mathbf{0} & \mathbf{0} & -\frac{\gamma_3}{2}\mathbf{I} & \mathbf{0} \\ \mathbf{0} & \mathbf{0} & \mathbf{0} & \mathbf{0} & \mathbf{0} \end{bmatrix}.$$

Note that γ_1, γ_2 and γ_3 are straightforward analysis parameters that can be adjusted as needed to ensure that $\mathbf{J}^\star$ is positive definite. These adjustments do not impact the performance of the controller.

References

Aracil, J., Acosta, J.A., Gordillo, F., 2013. A nonlinear hybrid controller for swinging-up and stabilizing the Furuta pendulum. Control engineering practice 21, 989–993.

Batista, P., Silvestre, C., Oliveira, P., 2011. On the observability of linear motion quantities in navigation systems. Systems & Control Letters 60, 101–110.

Hehn, M., D'Andrea, R., 2011. A flying inverted pendulum, in: 2011 IEEE International Conference on Robotics and Automation, IEEE. pp. 763–770.

Hofer, M., Muehlebach, M., D'Andrea, R., 2023. The One-Wheel Cubli: A 3D inverted pendulum that can balance with a single reaction wheel. Mechatronics 91, 102965.

Jazwinski, A.H., 2007. Stochastic processes and filtering theory. Courier Corporation.

Jin, W., Wang, Z., Yang, Z., Mou, S., 2020. Pontryagin differentiable programming: An end-to-end learning and control framework. Advances in Neural Information Processing Systems 33, 7979–7992.

Khalil, H.K., 2002. Nonlinear Systems. Pearson Education, Prentice Hall.

Khalil, H.K., 2017a. Cascade high-gain observers in output feedback control. Automatica 80, 110–118.

Khalil, H.K., 2017b. Extended high-gain observers as disturbance estimators. SICE Journal of Control, Measurement, and System Integration 10, 125–134.

Kocer, B.B., Tjahjowidodo, T., Pratama, M., Seet, G.G.L., 2019. Inspection-while-flying: an autonomous contact-based nondestructive test using UAV-tools. Automation in Construction 106, 102895.

Kong, L., Reis, J., He, W., Silvestre, C., 2023. Experimental validation of a robust prescribed performance nonlinear controller for an unmanned aerial vehicle with unknown mass. IEEE/ASME Transactions on Mechatronics .

Lee, T., 2017. Geometric control of quadrotor UAVs transporting a cable-suspended rigid body. IEEE Transactions on Control Systems Technology 26, 255–264.

Lee, T., Sreenath, K., Kumar, V., 2013. Geometric control of cooperating multiple quadrotor UAVs with a suspended payload, in: 52nd IEEE conference on decision and control, IEEE. pp. 5510–5515.

Liu, S., Fantoni, I., Chriette, A., 2024. Decentralized control and state estimation of a flying parallel robot interacting with the environment. Control Engineering Practice 144, 105817.

Martinez-Vasquez, A.H., Castro-Linares, R., Rodríguez-Mata, A.E., Sira-Ramírez, H., 2023. Spherical Inverted Pendulum on a Quadrotor UAV: A Flatness and Discontinuous Extended State Observer Approach. Machines 11, 578.

Raffo, G.V., Ortega, M.G., Madero, V., Rubio, F.R., 2015. Two-wheeled self-balanced pendulum workspace improvement via underactuated robust nonlinear control. Control Engineering Practice 44, 231–242.

Ran, M., Li, J., Xie, L., 2021. A new extended state observer for uncertain nonlinear systems. Automatica 131, 109772.

Yang, W., Yu, G., Reis, J., Silvestre, C., 2024. Robust nonlinear 3D control of an inverted pendulum balanced on a quadrotor. Automatica 159, 111336.

Yu, H., Li, X., Tao, Z., Feng, H., Zhang, S., Fu, Y., 2023. Hierarchical jumping optimization for hydraulic biped wheel-legged robots. Control Engineering Practice 141, 105721.

Zhang, C., Hu, H., Gu, D., Wang, J., 2017. Cascaded control for balancing an inverted pendulum on a flying quadrotor. Robotica 35, 1263–1279.

Zhao, J., Spong, M.W., 2001. Hybrid control for global stabilization of the cart–pendulum system. Automatica 37, 1941–1951.

Zhou, Y., Wang, A., Zhou, P., Wang, H., Chai, T., 2020. Dynamic performance enhancement for nonlinear stochastic systems using RBF driven nonlinear compensation with extended Kalman filter. Automatica 112, 108693.